

Thermally Activated Delayed Fluorescence Benzyl Cellulose Derivatives for Nondoped Organic Light-Emitting Diodes

Masaya Shibano, Hiroki Ochiai, Katsuaki Suzuki, Hiroshi Kamitakahara, Hironori Kaji, and Toshiyuki Takano*



Cite This: <https://dx.doi.org/10.1021/acs.macromol.9b02644>



Read Online

ACCESS |



Metrics & More

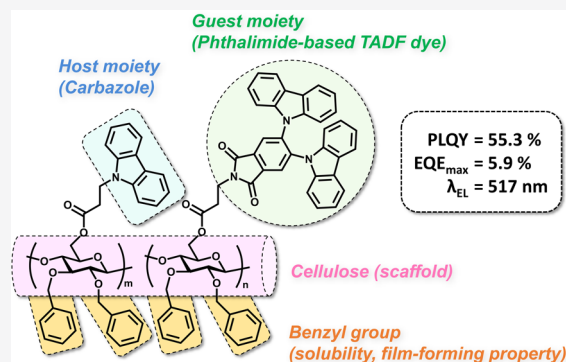


Article Recommendations



Supporting Information

ABSTRACT: Thermally activated delayed fluorescence (TADF) benzyl cellulose derivatives (TBC-X), which contained both carbazole (host) and phthalimide-based TADF dye (guest) moieties, were prepared from 2,3-di-O-benzyl cellulose in high yields. The TBC-X samples were soluble in common organic solvents such as CH₂Cl₂, CHCl₃, THF, and toluene. The photoluminescence spectra of TBC-X spin-coated films had a single emission peak derived only from guest moieties, which indicated efficient energy transfer from the host to guest moieties. The TBC-10 (with a content of host and guest moieties of 93 and 7, respectively) in a spin-coated film had the highest photoluminescence quantum yield of 55.3% and TADF characteristics. A nondoped organic light-emitting diode with TBC-10 as the emitting layer showed green emission ($\lambda_{EL} = 517$ nm) and achieved a maximum external quantum efficiency of 5.9%.



INTRODUCTION

Cellulose is the most abundant biomacromolecule in nature, and is important as biodegradable and renewable organic materials. Although cellulose and its derivatives are widely used in daily life, considerable attention has still been paid to the development of their value-added applications. One of the interesting proposals is an application of cellulose and its derivatives to green electronics.¹ For example, cellulose and its derivatives films have been reported to be applied to a biodegradable and transparent substrate of flexible organic light-emitting diodes (OLEDs).^{2–4} Another potential application to OLEDs is the use of cellulose derivative as a scaffold of the OLED elements in an emitting layer toward fully biodegradable OLEDs because the cellulose backbone is expected to inhibit aggregation of the elements as well as that of photosensitizer-bound cellulose derivatives toward biomaterial-based solar cells.^{5–8} Indeed, 6-O-[4-(9H-carbazol-9-yl)butyl]-2,3-di-O-methyl cellulose has been reported for a host material in the emitting layer of OLEDs.⁹ To develop cellulose-based OLED elements with high luminescence efficiency and low cost, in addition to inhibiting aggregation of elements, the following features are required. First is the use of thermally activated delayed fluorescence (TADF) dyes as an emitter.^{10–12} In OLEDs, holes and electrons are respectively injected from the cathode and anode and transferred into an emitting layer where they recombine to form excitons. The resulting excitons form as 25% singlet and 75% triplet excitons,¹³ however, only the former directly contributes to the electroluminescence (EL) in conventional fluorescence

OLEDs. Hence, early OLEDs using conventional fluorescence emitters had low luminescence efficiencies. Recently, to overcome this problem, OLEDs based on TADF dyes as emitters have been developed because triplet excitons can be converted to singlet excitons by a reverse intersystem crossing (RISC) in TADF dyes, resulting in 100% of excitons being available for electroluminescence.^{14–16} Therefore, the incorporation of TADF emitter to the cellulose molecule is essential for highly efficient OLEDs. Second is solution processability as described earlier.^{17–21} There are two fabrication methods for thin organic layers in OLEDs, that is, vacuum vapor deposition and solution processing methods. The former has been applied in many OLEDs with high performance manufacturing but requires complex processing and special manufacturing apparatus, which adds to the manufacturing costs. The latter method has several advantages, such as simple processing such as spin coating and inkjet printing, compatibility with flexible substrate such as cellulose films, and scalability to large-area flexible displays, which lower the fabrication costs of OLEDs. However, most of TADF emitters with low molecular weight for vacuum vapor deposition method tend to have low solubility, high crystallinity, and low film formability and thus

Received: December 13, 2019

Revised: March 14, 2020

are incompatible with solution processing methods, and in this aspect, polymeric materials such as cellulose derivative are favorable for the solution process. Finally, consideration should be given to materials capable of achieving nondoped OLEDs.^{22–30} Generally, guest materials should be doped with host materials to prevent concentration quenching in the emitting layer of the OLEDs. However, the doping process complicates the manufacturing process, resulting in high manufacturing costs. Therefore, self-host-type emitters that contain both host and guest moieties in the same molecule are required for nondoped OLEDs. However, there have been a few reports on self-host-type TADF pendant polymers,^{26–29} and further investigations for nondoped OLEDs are still required to reach the performance of doped devices.³⁰

In this study, 2,3-di-*O*-benzyl cellulose derivatives with host (carbazolyl groups: Cz groups) and guest (biscarbazolyl phthalimide ethyl ester groups: BCz-PI groups) moieties in the molecule, namely, a TADF-benzyl cellulose derivative (TBC-X) was designed as a self-host-type TADF cellulose derivative, as shown in Figure 1. The Cz group was selected for

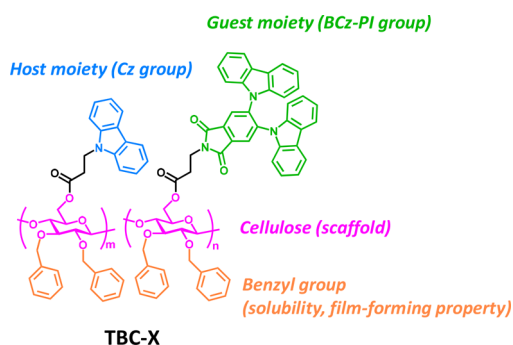


Figure 1. Molecular design of TADF benzyl cellulose derivative (TBC-X).

the host moieties because carbazole derivatives are the most common host materials in OLEDs.³¹ The BCz-PI group was also used as a guest moiety because BCz-PI-Ph is a TADF dye with high luminescence efficiency (Scheme 1), and it has been synthesized by a simple synthetic route.³² At first, 2,3-di-*O*-acetyl cellulose, a popular cellulose derivative, was considered as the scaffold; however, preliminary experiments showed that its solubility was very poor in common organic solvents. Hence, 2,3-di-*O*-benzyl cellulose (BnC) was selected as a

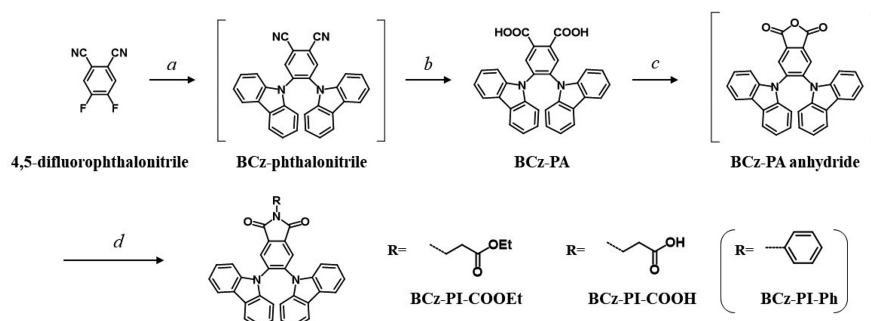
scaffold material because of its good solubility and film-forming properties. This paper describes the preparation of TBC-X, its application as the solution-processed emitting layer of OLEDs, and the evaluation of TADF characteristics of the system.

EXPERIMENTAL SECTION

Measurements. Fourier-transform infrared (FT-IR) spectra were recorded in KBr pellets with a Shimadzu IRPrestige-21 spectrophotometer (Shimadzu, Kyoto, Japan). ¹H and ¹³C NMR spectra were recorded on a Varian FT-NMR (500 MHz) spectrometer (Agilent Technologies, Santa Clara, CA). The chemical shift (δ) and coupling constant (J) are reported in parts per million (ppm) and hertz (Hz), respectively. Matrix-assisted laser desorption/ionization time-of-flight mass spectroscopy (MALDI-TOF MS) was recorded on a Bruker Autoflex III (Bruker Daltonics, Bremen, Germany) by using 2,5-dihydroxybenzoic acid as the matrix. Gel permeation chromatography (GPC) was performed on a Tosoh HLC-8220 GPC apparatus equipped with a refractive index detector under the following conditions—columns: two TSK Super HZM-H columns (Tosoh, Tokyo, Japan) connected in a series; flow rate: 0.25 mL min⁻¹; column temperature: 40 °C; eluent: THF; standards: polystyrene standards (TSK polystyrene standard, Tosoh). Differential scanning calorimetry (DSC) thermograms were recorded on a Mettler Toledo DSC823^e instrument (Mettler Toledo, Zurich, Switzerland) at a heating rate of 10 °C min⁻¹ under a nitrogen atmosphere. Atomic force microscope (AFM) observations of the spin-coated films were performed in dynamic mode with the use of a Shimadzu SPM-9600 system (Shimadzu) equipped with a tetrahedral-shaped silicon cantilever (AC240TS-C2, Olympus, Tokyo, Japan). Cyclic voltammetry was performed on an ALS/[H] CH Instruments electrochemical analyzer (Model 600E, BAS, Tokyo, Japan) using a conventional three-electrode configuration: a platinum electrode as the working electrode, a platinum wire as the counter electrode, and Ag/AgNO₃ as the reference electrode. Ferrocene (Fc) was added as an internal reference after each measurement, and all potentials were referenced to the ferrocenium/ferrocene (Fc⁺/Fc) couple. Photoluminescence (PL) spectra were recorded on a Shimadzu RF-5300 PC (Shimadzu) and a Horiba FluoroMax-4 (Horiba Scientific, Kyoto, Japan). UV–vis spectra were recorded on a Jasco V-560 (Jasco, Hachioji, Japan). Emission lifetimes were recorded on a Hamamatsu Photonics Quantaaurus-Tau C11367-01 (Hamamatsu Photonics, Hamamatsu, Japan). Photoluminescence quantum yields (PLQYs) were recorded on a Hamamatsu Photonics Quantaaurus-QY C11347-01 (Hamamatsu Photonics), and the PLQY measurements of spin-coated films were conducted under a stream of nitrogen.

Materials. The 2,3-di-*O*-benzyl cellulose (BnC) with a degree of substitution (DS) of benzyl groups of 1.98 (as calculated from the ¹H NMR spectrum) was synthesized according to a previously reported method.^{8,33,34} All other chemicals were purchased from commercial sources and used without further purification.

Scheme 1. Synthetic Routes to BCz-PI-COOEt, and BCz-PI-COOH



(a) Carbazole, K₂CO₃ / DMSO / 150 °C, 12 h. (b) KOH / EtOH:H₂O=1:1 / 105 °C, overnight. (c) Ac₂O / 140 °C, 2 h
(d) β -Alanine ethyl ester HCl, EDC HCl, Et₃N / dry DMF / r.t., 15 min \rightarrow 100 °C, overnight for BCz-PI-COOEt
 β -Alanine / AcOH / reflux, overnight for BCz-PI-COOH

Synthesis of a Model Compound (BCz-PI-COOEt) of TADF-Benzyl Cellulose Derivatives (TBC-X). 4,5-Bis(9H-carbazol-9-yl)phthalic Acid (BCz-PA). Carbazole (2.037 g, 12.2 mmol) and K_2CO_3 (3.367 g, 24.4 mmol) were added to DMSO (18 mL). After the mixture was stirred at room temperature (rt) for 0.5 h, 4,5-difluorophthalonitrile (1.0 g, 6.1 mmol) was added. The reaction mixture was stirred at 150 °C for 12 h, cooled to rt, and poured into distilled water (150 mL) at 0 °C. The resulting precipitate was collected by filtration with distilled water and extracted twice with CH_2Cl_2 . The combined organic layer was washed twice with brine, dried over anhydrous Na_2SO_4 , and concentrated *in vacuo*. The residue and KOH (1.683 g, 30 mmol) was added to EtOH/ H_2O (1/1, v/v, 30 mL). The reaction mixture was stirred at 105 °C overnight with a trap to neutralize a generated ammonia gas and filtrated with EtOH immediately. The filtrate was weakly acidified (pH: 4–5) with a 1 M hydrochloric acid. The resulting precipitate was collected by filtration with distilled water, thoroughly washed with distilled water, and recrystallized from EtOH to give BCz-PA as a dark yellow crystal (1.456 g, 48.1% yield). 1H NMR (DMSO- d_6): δ 8.14 (s, 2H), 7.94–7.92 (m, 4H), 7.26 (dd, 4H, $J = 7.0, 1.5$), 7.11–7.08 ppm (m, 8H) (Figure S1). ^{13}C NMR (DMSO- d_6): δ 167.3, 139.2, 135.5, 133.8, 130.8, 126.0, 123.1, 120.6, 120.4, 109.7 ppm (Figure S2). FT-IR (KBr): ν 3053, 1724, 1697, 1595, 1554, 1520, 1489, 1479, 1452, 1449, 1445, 1422, 1375, 1335, 1312, 1225, 746, 725 cm^{-1} . MALDI-TOF MS: m/z calcd for $C_{32}H_{20}N_2O_4$ 496.14; found 519.38 as $[M + Na]^+$.

3-(4,5-Bis(9H-carbazol-9-yl)phthalimide)propionic Acid Ethyl Ester (BCz-PI-COOEt). The mixture of BCz-PA (200 mg, 0.403 mmol) and Ac_2O (3 mL) was stirred at 140 °C for 2 h, concentrated, and dried *in vacuo*. The residue was dissolved in dry DMF (2 mL). β -Alanine ethyl ester hydrochloride (62 mg, 0.403 mmol) and Et_3N (0.22 mL, 1.61 mmol) were added to the solution. After stirring at rt for 15 min, 1-(3-(dimethylamino)propyl)-3-ethylcarbodiimide hydrochloride (EDC-HCl) (77 mg, 0.403 mmol) was added to the solution. The solution was stirred at 100 °C overnight and concentrated. The residue was purified by preparative thin-layer chromatography (PTLC) with the use of silica gel glass plates coated with silica gel 60 PF₂₅₄ (Merck, Darmstadt, Germany) with 2 mm thickness (eluent: EtOAc/*n*-hexane = 1/2, v/v) to afford BCz-PI-COOEt as a yellow solid (108 mg, 46.7% yield). 1H NMR ($CDCl_3$): δ 8.36 (s, 2H), 7.79–7.78 (m, 4H), 7.12–7.03 (m, 12H), 4.21 (d, 1H, $J = 7.0$), 4.18 (d, 1H, $J = 7.0$), 4.12 (t, 2H, $J = 7.0$), 2.83 (t, 2H, $J = 7.0$), 1.29 (t, 3H, $J = 7.0$) ppm (Figure S3). ^{13}C NMR ($CDCl_3$): δ 170.7, 166.6, 139.1, 138.8, 131.2, 125.8, 125.5, 124.0, 120.9, 120.1, 109.4, 61.0, 34.3, 32.9, 14.2 ppm (Figure S4). FT-IR (KBr): ν 3055, 2980, 1776, 1734, 1715, 1618, 1597, 1497, 1479, 1449, 1396, 1375, 1335, 1312, 1233, 1198, 746, 723 cm^{-1} . MALDI-TOF MS: m/z calcd for $C_{37}H_{27}N_3O_4$ 577.20; found 577.32 as $[M]^+$.

The highest occupied molecular orbital (HOMO), the lowest unoccupied molecular orbital (LUMO), and the difference between S_1 and T_1 (ΔE_{ST}) of BCz-PI-COOEt were calculated by using density functional theory (DFT) and time-dependent DFT with the Gaussian 16 program package at the PBE0/6-31G(d) level.

Synthesis of TADF-Benzyl Cellulose Derivatives (TBC-X). 3-(9H-Carbazol-9-yl)propionic Acid (Cz-COOH) (Host Dye Part). Carbazole (6.0 g, 35.8 mmol) and NaOH (4.308 g, 107.7 mmol) were added to DMSO (30 mL). After the mixture was stirred at 85 °C for 0.5 h, methyl 3-bromopropionate (4.7 mL, 43.1 mmol) was added. The reaction mixture was then stirred at 85 °C overnight. Distilled water (0.5 mL) was added to the mixture. After 10 min, the reaction mixture was poured into distilled water (200 mL) at 0 °C. The pH of the solution was adjusted to be in the range of 3–4 with 1 M hydrochloric acid. The resulting precipitate was collected by filtration with distilled water, washed with distilled water, and recrystallized from EtOH to give a colorless crystal (6.71 g, 78.0% yield). 1H NMR (CD_3OD): δ 8.05 (dd, 2H, $J = 7.5, 1.0$), 7.52 (broad d, 2H, $J = 8.5$), 7.43 (ddd, 2H, $J = 7.5, 7.0, 1.0$), 7.18 (ddd, 2H, $J = 7.5, 7.0, 1.0$), 4.65 (t, 2H, $J = 7.0$), 2.80 (t, 2H, $J = 7.0$) ppm (Figure S5). ^{13}C NMR (CD_3OD): δ 175.1, 141.4, 126.8, 124.3, 121.1, 120.1, 109.9, 39.8, 34.3 ppm (Figure S6). FT-IR (KBr): ν 3049, 1709, 1705, 1701, 1593,

1485, 1464, 1450, 1352, 1327, 1279, 1248, 1240, 1231, 1198, 1153, 754, 727 cm^{-1} . MALDI-TOF MS: m/z calcd for $C_{15}H_{13}NO_2$ 239.09; found 239.18 as $[M]^+$.

3-(4,5-Bis(9H-carbazol-9-yl)phthalimide)propionic Acid (BCz-PI-COOH) (Guest Dye Part). The mixture of BCz-PA (200 mg, 0.403 mmol) and Ac_2O (3 mL) was stirred at 140 °C for 2 h, concentrated, and dried *in vacuo*. The residue and β -alanine (36 mg, 0.403 mmol) were added to AcOH (2 mL), and the reaction mixture was stirred under reflux overnight, concentrated, and purified by PTLC with the use of a silica gel plate as described above (eluent: MeOH/ CH_2Cl_2 = 1/9, v/v) to give BCz-PI-COOH as a yellow solid (161 mg, 72.5% yield). 1H NMR (DMSO- d_6): δ 8.32 (s, 2H), 7.94–7.90 (m, 4H), 7.27–7.25 (m, 4H), 7.10–7.06 (m, 8H), 3.88 (broad t, 2H, $J = 8.0$), 2.56 (t, 2H, $J = 7.0$) ppm. ^{13}C NMR (DMSO- d_6): δ 166.4, 139.0, 138.5, 132.0, 125.8, 125.3, 123.1, 120.6, 120.3, 109.7, 34.5, 33.4 ppm. FT-IR (KBr): ν 3466, 3059, 1775, 1713, 1616, 1597, 1497, 1479, 1449, 1396, 1335, 1312, 1233, 746, 723 cm^{-1} . MALDI-TOF MS: m/z calcd for $C_{35}H_{23}N_3O_4$ 549.17, found 549.19 as $[M]^+$.

TADF-Benzyl Cellulose Derivatives (TBC-X). Typical Method. BnC was dissolved in DMF/ $CHCl_3$ (1/1, v/v) (2 mL). Cz-COOH, BCz-PI-COOH, *N,N'*-diisopropylcarbodiimide (DIC), and 4-(dimethylamino)pyridine (DMAP) were added to the solution in this order. After being stirred at 30 °C for 48 h, the reaction solution was added dropwise into MeOH (100 mL). The resulting precipitate was collected by filtration with MeOH, washed with MeOH, and dissolved in a small amount of $CHCl_3$. The solution was added dropwise to the MeOH again. The resulting precipitate was collected by filtration with MeOH, washed with MeOH, and dried *in vacuo* to obtain TBC-X. The feed molar ratio of Cz-COOH (host)/BCz-PI-COOH (guest) was 100/0 (for TBC-0, control), 90/10 (for TBC-10), 85/15 (for TBC-15), and 80/20 (for TBC-20).

The DS of host and guest moieties of TBC-X were respectively determined according to eqs 1 and 2 with the use of 1H NMR spectra data

$$DS_{\text{host}} = \frac{5D(2A - B)}{2(-6A - 3B + 2C)} \quad (1)$$

$$DS_{\text{guest}} = \frac{5BD}{2(-6A - 3B + 2C)} \quad (2)$$

where A is total integrated values of aromatic-H signals of guest and host moieties (7.80–8.20 ppm), B is the integrated value of aromatic-H signals of host moieties (7.60–7.80 ppm), C is the total integrated values of aromatic-H signals of guest moieties, host moieties, and benzyl groups (6.60–7.60 ppm), and D is the DS of benzyl groups of BnC.

TBC-0 (Control). BnC (30 mg, 0.0876 mmol), Cz-COOH (63 mg, 0.26 mmol), DIC (41 μ L, 0.26 mmol), and DMAP (32 mg, 0.26 mmol) were used to obtain TBC-0 (48 mg, 97.3%). DS_{host} : 1.03; M_n : 5.0×10^3 ($M_w/M_n = 2.8$). 1H NMR ($CDCl_3$): δ 8.00 (carbazole-H of Cz groups), 7.50–6.60 (carbazole-H of Cz groups, aromatic-H of benzyl groups), 5.30–2.80 (ring-H of Cell, benzyl-H, $-N-CH_2-CH_2-$ of Cz groups), 2.44 ($-N-CH_2-CH_2-$ of Cz groups) ppm (Figure S7). ^{13}C NMR ($CDCl_3$): δ 170.5 (C=O), 138.8, 137.9, 128.2, 128.0, 127.4, 127.0, 125.7, 122.9, 120.4, 119.2, 108.4, 103.1 (C-1), 82.7 (C-3), 81.5 (C-2), 78.8, 76.0–72.0 (C-4, C-5, benzyl-C), 63.4 (C-6), 38.3, 33.0 ppm. FT-IR (KBr): ν 3445, 3028, 2874, 1740, 1628, 1597, 1485, 1462, 1454, 1350, 1325, 1229, 1211, 1169, 1153, 1065, 1028, 750, 725, 698 cm^{-1} (Figure S8).

TBC-10. BnC (40 mg, 0.117 mmol), Cz-COOH (50.3 mg, 0.21 mmol), BCz-PI-COOH (12.9 mg, 0.023 mmol), DIC (36 μ L, 0.23 mmol), and DMAP (28.5 mg, 0.23 mmol) were used to obtain TBC-10 (57.3 mg, 88.0%). DS_{host} : 0.82, DS_{guest} : 0.06; M_n : 5.0×10^3 ($M_w/M_n = 3.0$). 1H NMR ($CDCl_3$): δ 8.10 (aromatic-H of BCz-PI groups), 7.99 (carbazole-H of Cz groups), 7.73 (carbazole-H of BCz-PI groups), 7.50–6.60 (carbazole-H of BCz-PI and Cz groups, aromatic-H of benzyl groups), 5.30–2.80 (ring-H of Cell, benzyl-H, $-N-CH_2-CH_2-$ of BCz-PI and Cz groups), 2.76 ($-N-CH_2-CH_2-$ of BCz-PI groups), 2.44 ppm ($-N-CH_2-CH_2-$ of Cz groups) (Figure

S7). ^{13}C NMR (CDCl_3): δ 170.5 (C=O), 166.2 (imide C=O), 140.0, 139.7, 138.8, 137.9, 128.2, 128.0, 127.4, 125.7, 123.9, 122.9, 120.8, 120.4, 119.2, 109.3, 108.4, 103.2 (C-1), 82.7 (C-3), 81.6 (C-2), 78.9, 76.0–72.0 (C-4, C-5, benzyl-C), 63.1 (C-6), 38.3, 33.0 ppm. FT-IR (KBr): ν 3445, 3028, 2870, 1740, 1717, 1626, 1597, 1485, 1462, 1454, 1348, 1325, 1231, 1211, 1169, 1153, 1063, 1028, 750, 723, 698 cm^{-1} (Figure S8).

TBC-15. BnC (40 mg, 0.117 mmol), Cz-COOH (47.5 mg, 0.20 mmol), BCz-PI-COOH (19.3 mg, 0.035 mmol), DIC (36 μL , 0.23 mmol), and DMAP (28.5 mg, 0.23 mmol) were used to obtain TBC-15 (60.2 mg, 93.2%). DS_{host} : 0.74, DS_{guest} : 0.09; M_n : 5.6×10^3 ($M_w/M_n = 2.7$). ^1H NMR (CDCl_3): δ 8.10 (aromatic-H of BCz-PI groups), 7.99 (carbazole-H of Cz groups), 7.73 (carbazole-H of BCz-PI groups), 7.50–6.60 (carbazole-H of BCz-PI and Cz groups, aromatic-H of benzyl groups), 5.30–2.80 (ring-H of Cell, benzyl-H, $-\text{N}-\text{CH}_2-\text{CH}_2-$ of BCz-PI and Cz groups), 2.75 ($-\text{N}-\text{CH}_2-\text{CH}_2-$ of BCz-PI groups), 2.44 ppm ($-\text{N}-\text{CH}_2-\text{CH}_2-$ of Cz groups) (Figure S7). ^{13}C NMR (CDCl_3): δ 170.5 (C=O), 166.3 (imide C=O), 139.9, 139.7, 138.8, 138.0, 129.6, 128.2, 128.0, 127.4, 125.7, 123.9, 122.9, 120.9, 120.4, 120.1, 119.2, 109.3, 108.6, 108.4, 103.1 (C-1), 82.8 (C-3), 81.7 (C-2), 78.9, 76.0–72.0 (C-4, C-5, benzyl-C), 63.3 (C-6), 38.3, 33.0 ppm. FT-IR (KBr): ν 3464, 3028, 2870, 1738, 1717, 1625, 1597, 1495, 1485, 1454, 1348, 1325, 1231, 1213, 1169, 1155, 1061, 1028, 748, 723, 696 cm^{-1} (Figure S8).

TBC-20. BnC (40 mg, 0.117 mmol), Cz-COOH (44.7 mg, 0.187 mmol), BCz-PI-COOH (25.7 mg, 0.047 mmol), DIC (36 μL , 0.23 mmol), and DMAP (28.5 mg, 0.23 mmol) were used to obtain TBC-20 (59.8 mg, 87.2%). DS_{host} : 0.75, DS_{guest} : 0.15; M_n : 4.9×10^3 ($M_w/M_n = 3.0$). ^1H NMR (CDCl_3): δ 8.10 (aromatic-H of BCz-PI groups), 7.99 (carbazole-H of Cz groups), 7.73 (carbazole-H of BCz-PI groups), 7.50–6.60 (carbazole-H of BCz-PI and Cz groups, aromatic-H of benzyl groups), 5.30–2.80 (ring-H of Cell, benzyl-H, $-\text{N}-\text{CH}_2-\text{CH}_2-$ of BCz-PI and Cz groups), 2.76 ($-\text{N}-\text{CH}_2-\text{CH}_2-$ of BCz-PI groups), 2.45 ppm ($-\text{N}-\text{CH}_2-\text{CH}_2-$ of Cz groups) (Figure S7). ^{13}C NMR (CDCl_3): δ 170.5 (C=O), 166.3 (imide C=O), 140.0, 139.7, 138.8, 137.9, 131.0, 129.6, 128.1, 128.0, 127.4, 125.7, 123.9, 122.9, 120.8, 120.4, 120.1, 119.2, 109.3, 108.5, 103.1 (C-1), 82.7 (C-3), 81.6 (C-2), 79.0, 76.0–72.0 (C-4, C-5, benzyl-C), 63.4 (C-6), 38.3, 33.0 ppm. FT-IR (KBr): ν 3466, 3028, 2870, 1740, 1717, 1626, 1597, 1497, 1485, 1452, 1348, 1325, 1231, 1213, 1169, 1153, 1061, 1028, 748, 723, 696 cm^{-1} (Figure S8).

Preparation of TBC-X Spin-Coated Films. Spin-coated films for respective measurements were fabricated as follows: For measurements of the PL spectra, a solution of TBC-X in CHCl_3 (10 mg mL^{-1}) was spin-coated on quartz glass (25 mm \times 25 mm) at 1000 rpm for 30 s. For the PLQYs measurements, a solution of TBC-X in toluene (15 mg mL^{-1}) was spin-coated on quartz glass (10 mm \times 15 mm) at 800 rpm for 30 s and used without encapsulation. For the PL lifetime measurements, a solution of TBC-10 in toluene (15 mg mL^{-1}) was spin-coated on quartz glass (30 mm \times 30 mm) at 800 rpm for 30 s and encapsulated with glass caps in a glovebox ($\text{O}_2 < 0.1$ ppm). For AFM imaging, a solution of TBC-10 in CHCl_3 (10 mg mL^{-1}) was spin-coated on a silicon wafer (10 mm \times 10 mm) at 1000 rpm for 30 s.

Fabrication and Evaluation of Devices Using TBC-10 as the Emitting Layer. Two devices containing an emitting layer of different thickness were fabricated (devices A and B). Before spin-coating, an indium tin oxide (ITO) substrate was cleaned as follows: (i) 10 min sonication in detergent, distilled water (two times), acetone, and 2-propanol; (ii) 5 min exposure to a hot steam of 2-propanol; (iii) UV- O_3 irradiation for 30 min. Next, poly(3,4-ethylenedioxythiophene)-poly(styrenesulfonate) (PEDOT:PSS, CLEVIOSTM AI 4083 (Heraeus, Hanau, German)) was spin-coated on the cleaned ITO substrate at 4000 rpm for 30 s and baked at 150 $^\circ\text{C}$ for 10 min under air. After 5 min of nitrogen flow for cooling, the emitting layer was formed at 800 rpm for 30 s from TBC-10–toluene solution (for device A: 15 mg mL^{-1} ; for device B: 25 mg mL^{-1}) upon the PEDOT:PSS layer. After baking at 50 $^\circ\text{C}$ for 30 min and cooling under a nitrogen stream, 4,6-bis[3,5-di(pyridine-4-yl)phenyl]-2-methylpyrimidine (B4PYMPM), lithium quinoline-8-olate (Liq),

and Al were formed by vacuum deposition using a deposition apparatus (SE-4260, ALS Technology, Sagami-hara, Japan) at a pressure of $<10^{-4}$ Pa to obtain devices with an active area of 4 mm^2 . Finally, the devices were encapsulated with glass caps, and getter films were attached to remove oxygen and moisture. The performances of devices A and B were recorded on a Hamamatsu Photonics C9920-12 (Hamamatsu Photonics) with a Keithley SourceMeter 2400 (Keithley Instruments, Cleveland, OH).

RESULTS AND DISCUSSION

Synthesis of a Model Compound (BCz-PI-COOEt) of TBC-X. BCz-PI dye moieties are important functional groups for TADF characteristics.³² However, preliminary experiments showed that triazole linkages between the cellulose backbone and BCz-PI moieties prevented the TADF characteristics of the BCz-PI moieties. Hence, the synthesis of BCz-PI-COOEt was investigated as a model compound of TBC-X to investigate the influence of ester linkages on the TADF characteristics.

First, the HOMO, LUMO, and ΔE_{ST} of BCz-PI-COOEt were calculated by density functional theory (DFT). The distributions of HOMO and LUMO energy densities of BCz-PI-COOEt are shown in Figure 2. The HOMO and LUMO of

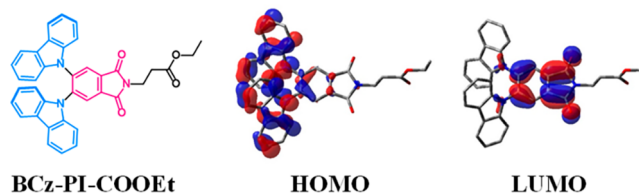


Figure 2. Chemical structure and HOMO/LUMO distribution of BCz-PI-COOEt calculated at the PBE0/6-31G(d) level.

BCz-PI-COOEt were mainly located at the carbazole and phthalimide moieties of BCz-PI-COOEt, respectively. The HOMO/LUMO energy levels and ΔE_{ST} were also calculated to be $-5.88/-2.36$ and 0.34 eV, respectively, suggesting that BCz-PI-COOEt was expected as a TADF dye.

BCz-PI-Ph, which is a TADF dye with high luminescence efficiency, has been synthesized from 4,5-difluorophthalic anhydride in two steps: namely, phenylphthalimide formation and condensation with carbazole.³² However, 4,5-difluorophthalic anhydride was not commercially available. Thus, BCz-PI-COOEt was synthesized from 4,5-difluorophthalonitrile by two reaction steps, as shown in Scheme 1. Condensation of 4,5-difluorophthalonitrile with carbazole in the presence of K_2CO_3 and subsequent alkali hydrolysis with KOH were performed to afford BCz-PA in 48.1% yield. This intermediate was further converted by reactions with Ac_2O and β -alanine ethyl ester hydrochloride to BCz-PI-COOEt in 46.7% yield. Characteristic signals assigned to aromatic-H of phthalimide moieties at 8.36 ppm, aromatic-H of carbazole moieties at 7.80–7.00 ppm, and methylene-H of $-\text{N}-\text{CH}_2-\text{CH}_2-\text{CO}-$ at 2.80 ppm were found in the ^1H NMR spectrum of BCz-PI-COOEt (Figure S3). In addition, the bands derived from ester C=O at 1734 cm^{-1} and from phthalimide C=O at 1715 cm^{-1} were also observed in the FT-IR spectrum of BCz-PI-COOEt. The measured $[M]^+$ value of BCz-PI-COOEt (577.32) agreed with its calculated value (577.20) in the MALDI-TOF MS spectrum. These results confirmed the successful synthesis of BCz-PI-COOEt. This synthetic method is also expected to be applicable to BCz-PI-based dyes other than BCz-PI-COOEt.

Figure 3A shows UV-vis and PL spectra of BCz-PI-COOEt. A peak derived from the intramolecular charge-transfer

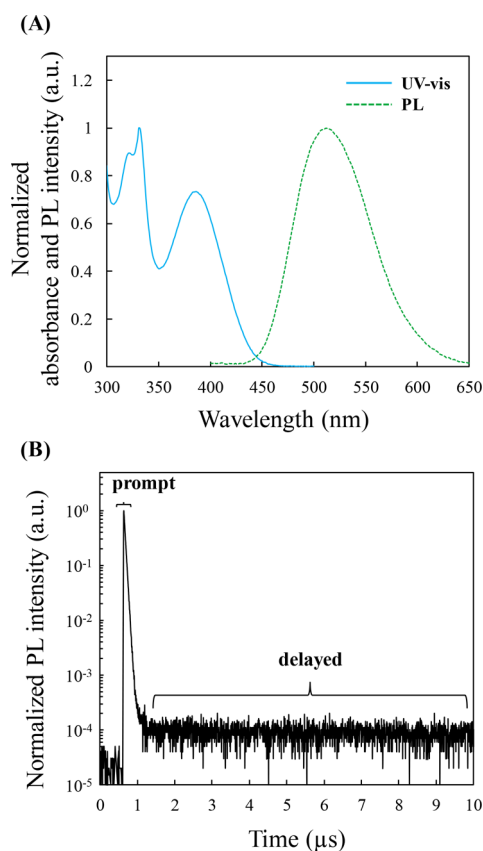


Figure 3. (A) UV-vis and PL spectra of BCz-PI-COOEt in toluene solution (1.0×10^{-5} M) (normalized at 331 nm: UV-vis, 512 nm: PL; excited at 330 nm in PL measurements). (B) Transient PL decay curve of BCz-PI-COOEt in toluene solution (0.01 mg mL $^{-1}$) at rt after 15 min degassing by argon.

transition from the HOMO to the LUMO at 386 nm was observed in the UV spectrum of BCz-PI-COOEt.^{32,35,36} An emission peak at 512 nm was also found in the PL spectrum of BCz-PI-COOEt, which corresponds to that at 510 nm of BCz-PI-Ph in the literature.³² These spectral results suggest the

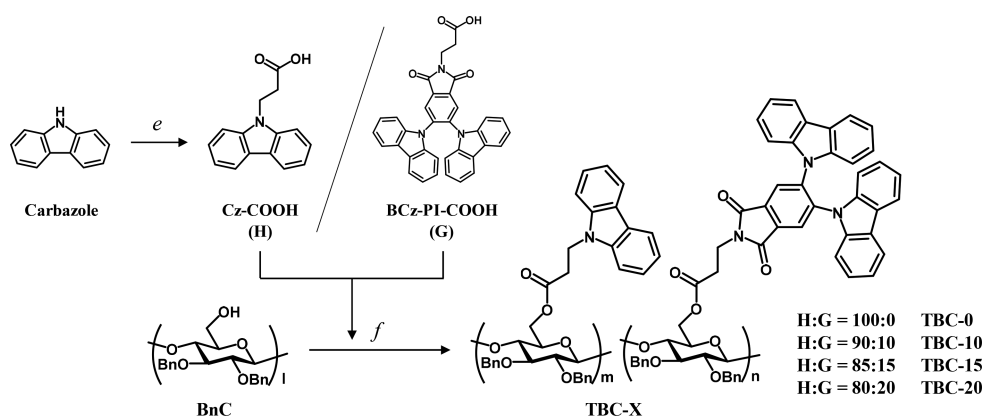
separation of HOMO and LUMO in BCz-PI-COOEt. Furthermore, a delayed component was observed in the transient PL decay curve of BCz-PI-COOEt, as shown in Figure 3B. The PLQY of BCz-PI-COOEt was 49.5% under argon bubbling. These results suggest that the ester linkage did not have a negative effect on the TADF characteristics of the BCz-PI moieties and that TBC-X might act as a TADF dye.

Synthesis of TADF Benzyl Cellulose Derivatives (TBC-X). First, host and guest dye parts of TBC-X, that is, Cz-COOH and BCz-PI-COOH, were synthesized to introduce host and guest dye moieties into the cellulose backbone through ester linkages. Cz-COOH was synthesized by the reaction of carbazole with methyl 3-bromopropionate in 78.0% yield. The measured value of $[M]^+$ of Cz-COOH (239.09) agreed with its calculated value of $[M]^+$ (239.18) in the MALDI-TOF MS spectrum. BCz-PI-COOH was also synthesized from BCz-PI-PA according to a modified synthetic method for BCz-PI-COOEt with the use of β -alanine instead of β -alanine ethyl ester hydrochloride in 72.5% yield. The measured value of $[M]^+$ of BCz-PI-COOH (549.19) agreed with its calculated value of $[M]^+$ (549.17) in the MALDI-TOF MS spectrum.

Next, TADF-benzyl cellulose derivatives (TBC-0, -10, -15, and -20) were synthesized by a Steglich-type esterification of BnC with different feed molar ratios of Cz-COOH (host dye part)/BCz-PI-COOH (guest dye part) of 100/0, 90/10, 85/15, and 70/30, respectively (Scheme 2). TBC-0 was selected as a cellulose derivative having only host moieties for comparison with TBC-10, -15, and -20.

Figures 4 and 5 show FT-IR and ^1H NMR spectra of BnC, TBC-0, and TBC-10. The characteristic band assigned to hydroxy groups at 3445 cm $^{-1}$ decreased, and bands assigned to host moieties (Cz groups) at 1628 , 1597 , and 750 cm $^{-1}$ and ester bonds at 1740 cm $^{-1}$ appeared in the FT-IR spectra of TBC-0 and TBC-10, indicating that host moieties were introduced into the cellulose backbone through ester linkages in TBC-0 and TBC-10. This is also supported by the appearance of the new signals assigned to aromatic-H (H_a) of host moieties at 8.00 ppm and to methylene-H (H_f) of spacer of host moieties at 2.44 ppm in ^1H NMR spectra of TBC-0 and TBC-10. However, the characteristic band assigned to imide bonds of guest moieties (BCz-PI groups) at 1717 cm $^{-1}$ and signals assigned to aromatic-H (H_g) of guest moieties at

Scheme 2. Synthetic Route to TADF Benzyl Cellulose Derivatives (TBC-X)



(e) 1) Methyl 3-bromopropionate, NaOH / DMSO / 85°C, overnight; 2) H₂O / 85°C, 10min
(f) Cz-COOH (H) / BCz-PI-COOH (G), DIC, DMAP / DMF:CHCl₃ (1:1, v:v) / 30°C, 48 h.

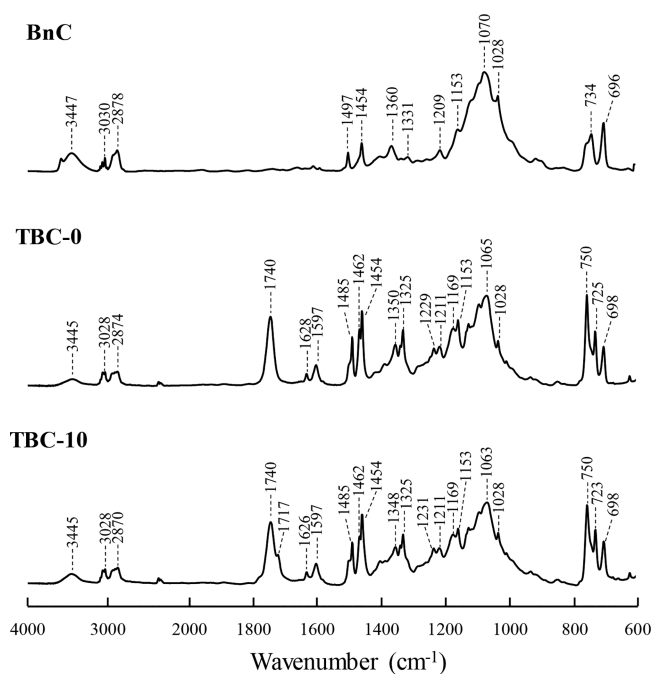


Figure 4. FT-IR spectra of BnC, TBC-0, and TBC-10.

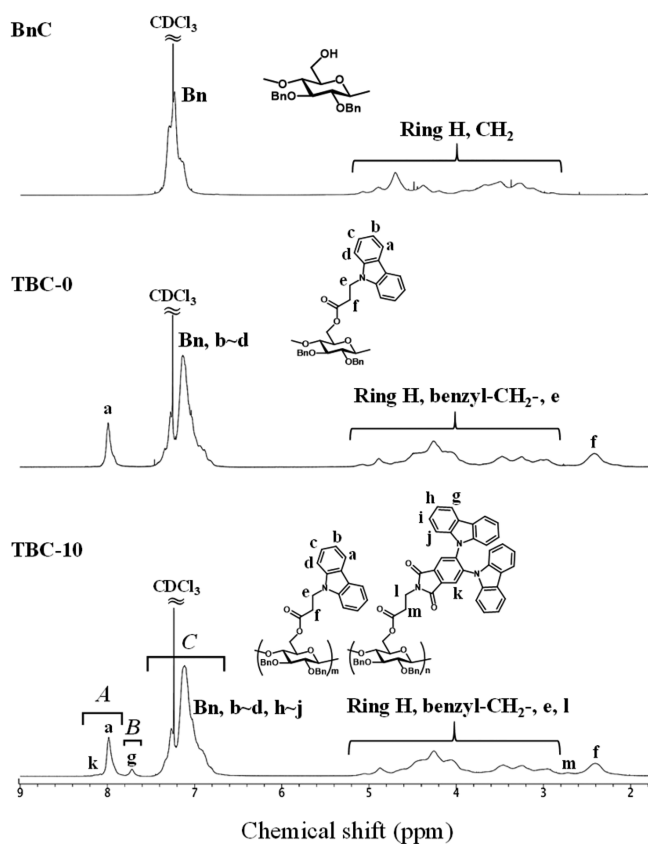


Figure 5. ^1H NMR spectra of BnC, TBC-0, and TBC-10.

7.73 ppm and methylene-H (H_m) of the spacer of guest moieties at 2.76 ppm were also observed in the FT-IR and ^1H NMR spectra of TBC-10, respectively. Furthermore, a peak derived from guest moieties at 390 nm was also observed and increased in the UV-vis spectra of TBC-X as the molar feed ratio of guest moieties was increased (Figure 6A). These

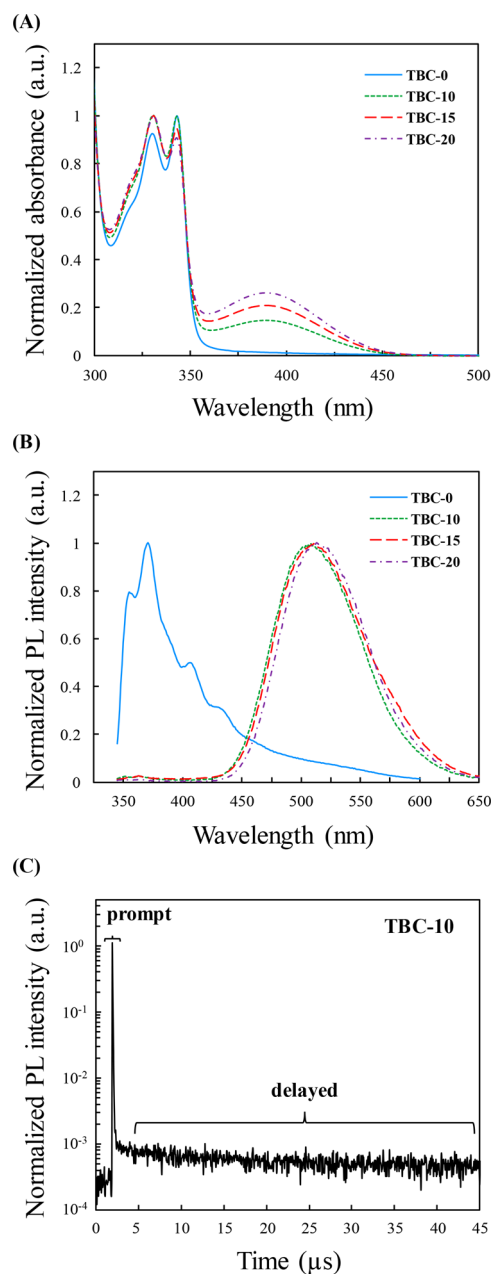


Figure 6. (A) UV-vis spectra of TBC-X in toluene solution (0.01 mg mL^{-1}) (normalized at 343 nm). (B) PL spectra of TBC-X in the neat films (normalized at peak top, excited at 330 nm). (C) transient PL decay curve of TBC-10 in the neat film at 25°C .

results indicate that TBC-10 had both host and guest moieties through ester linkages. The number-averaged molecular weight (M_n) of TBC-10 was 5000. The DS values of host and guest moieties of TBC-X, simply determined by the ^1H NMR spectra method described above, were respectively 1.03 and 0 for TBC-0, 0.82 and 0.06 for TBC-10, 0.74 and 0.09 for TBC-15, and 0.75 and 0.15 for TBC-20. The content ratios of host and guest moieties in TBC-X were 100/0 in TBC-0, 93/7 in TBC-10, 89/11 in TBC-15, and 84/16 in TBC-20, respectively, as shown in Table 1. Although these results suggest that the reactivity of BCz-PI-COOH was somewhat lower than that of Cz-COOH, the feed molar ratios of Cz-COOH and BCz-PI-COOH in the preparations were

Table 1. Characterization Data of TBC-X

samples	feed molar ratio ^a	DS of host/guest (total)	ratio of host and guest	M_n	T_g (°C)	λ_{abs}^b (nm)	λ_{PL}^c (nm)	PLQY ^d (%)
TBC-0	100/0	1.03/0 (1.03)	100/0	5.0×10^3	85.1	330, 343	355, 371, 401, 432	
TBC-10	90/10	0.82/0.06 (0.88)	93/7	5.0×10^3	91.7	331, 343, 390	508	55.3
TBC-15	85/15	0.74/0.09 (0.83)	89/11	5.6×10^3	95.4	331, 343, 390	511	53.7
TBC-20	80/20	0.75/0.15 (0.90)	84/16	4.9×10^3	100.7	331, 343, 390	513	46.5

^aFeed molar ratio of Cz-COOH/BCz-PI-COOEt. ^bMeasured in toluene solution at rt. ^cMeasured in the neat film. ^dMeasured in the neat film under nitrogen condition.

Table 2. Evaluation Results of the Performances of Devices A and B

device	conc ^a (mg mL ⁻¹)	V_{on}^b (V)	λ_{EL}^c (nm)	CE_{max} (cd A ⁻¹)	PE_{max} (lm W ⁻¹)	EQE_{max} (%)	CIE^d (x, y)
A	15	3.7	516	5	3.8	1.7	(0.30, 0.51)
B	25	3.6	517	17.6	13.9	5.9	(0.30, 0.51)

^aConcentration of TBC-10 in toluene solution. ^bThe driving voltage at 1 cd m⁻². ^cEL emission peak at 5 V. ^dCIE coordinate at 5 V.

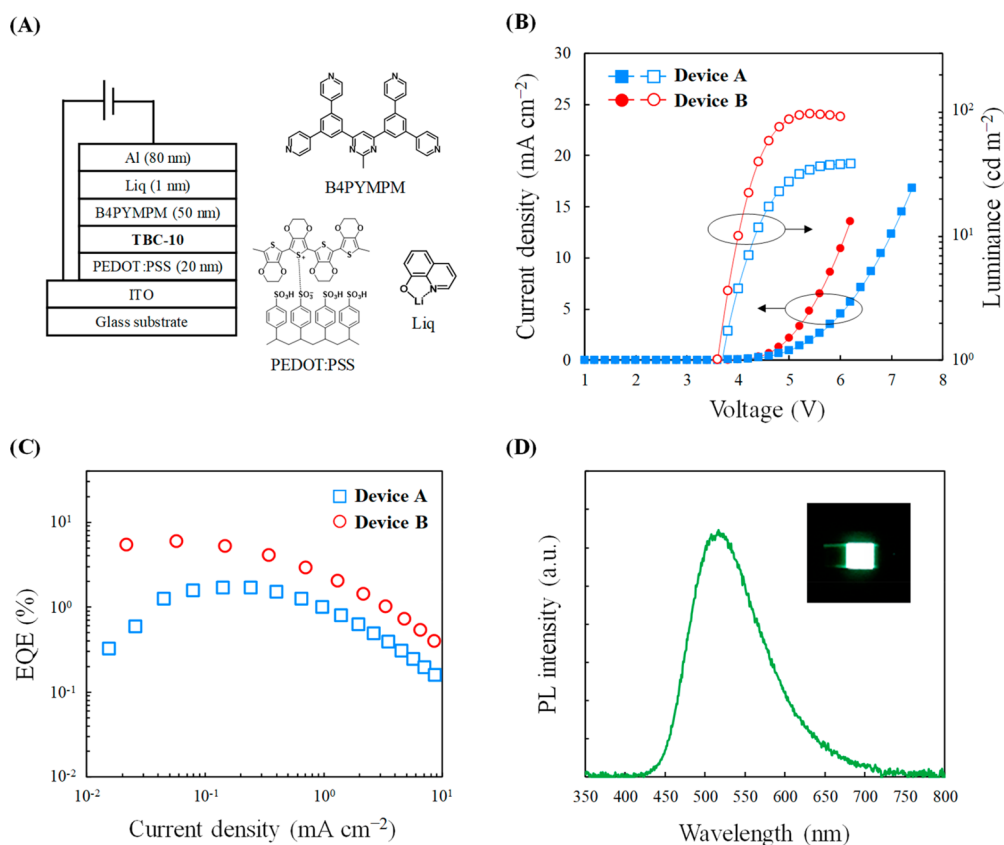


Figure 7. (A) Structure of devices based on TBC-10 as the emitting layer and chemical structures of other materials. (B) Current density–voltage–luminance characteristics of the devices. (C) EQE vs current density characteristics of the devices. (D) EL spectrum of device B at 5 V. Inset: luminescent image of device B.

approximately reflected by those of the content ratio of host and guest moieties in TBC-X.

Physical and Optical Properties of TADF Benzyl Cellulose Derivatives (TBC-X). TBC-X was soluble in CH₂Cl₂, CHCl₃, THF, and toluene, suggesting that BnC contributed to improved solubility of the BCz-PI-based dye moieties as expected. Next, a spin-coated film of TBC-10 was fabricated on mica as a representative sample to evaluate the film-forming properties of TBC-X and observed by AFM. The surface was smooth and homogeneous in AFM height and phase images of the film (Figure S9), suggesting that TBC-X had good film-forming properties. The glass transition temperatures (T_g) of TBC-X increased as the feed molar

ratio of guest moieties was increased (85.1–100.7 °C) (Table 1 and Figure S10). The electrochemical behavior of TBC-X in CH₂Cl₂ was also investigated by cyclic voltammetry (CV) (Figure S11). The oxidation peak was observed clearly in the CV of TBC-10 and -15. It was estimated from the CV that HOMO/LUMO of TBC-10 and TBC-15 were -5.79 eV/ -2.96 eV and -5.72 eV/ -2.92 eV, respectively.

Figure 6B shows the PL spectra of the TBC-X films (excitation wavelength: 330 nm), which were fabricated on quartz glasses by spin-coating. Multimodal emission peaks assigned to host moieties (355, 371, 401, and 432 nm) were observed in the PL spectrum of the TBC-0 film. The emission from host moieties was almost suppressed in the PL spectra of

the TBC-10, -15, and -20 films, although the emission was clearly observed in the PL spectra of the TBC-10, -15, and -20 toluene solution (Figure S12). Single emission peaks assigned to guest moieties were observed at 508, 511, and 513 nm in the PL spectra of the TBC-10, -15, and -20 films, respectively. The peaks red-shifted slightly as the guest moiety ratio was increased. These results suggested the efficient energy transfer from the host moieties to guest moieties in the TBC-10, -15, and -20 films.

Next, the TBC-10, -15, and -20 films were subjected to PLQY measurements under a nitrogen atmosphere. The PLQY values of the TBC-10, -15, and -20 films were 55.3%, 53.7%, and 46.5%, respectively, which were almost equal to those of self-host-type TADF pendant polymer films in the literature.^{26–28} The TBC-10 film showed the best performance among them. Furthermore, long-delayed components were clearly observed in the transient PL decay curve of the TBC-10 film, as shown in Figure 6C, suggesting that conversion from singlet to triplet excitons proceeded smoothly in the TBC-10 film; namely, TBC-10 had TADF characteristics. These results suggest that TBC-X might be a promising material for solution-processed OLEDs.

Fabrication and Evaluation of the Devices on the Basis of TBC-10 as the Emitting Layer. Two nondoped OLEDs using TBC-10 as an emitting layer (devices A and B) were fabricated and evaluated (Table 2). The emitting layers of devices A and B were fabricated from TBC-10 in toluene solutions with 15 and 25 mg mL⁻¹, respectively, by spin-coating. The device structures were [ITO (50 nm)/PEDOT:PSS (20 nm)/TBC-10/B4PYMPM (50 nm)/Liq (1 nm)/Al (80 nm)], as shown in Figure 7A.

Figure 7B shows the current density–voltage–luminance (J – V – L) characteristics. The driving voltages at 1 cd m⁻² were 3.7 and 3.6 V in devices A and B, respectively. The maximum current efficiency (CE), power efficiency (PE), and EQE values of device B were higher than those of device A (Figure S13 and Figure 7C), suggesting that more efficient recombination of holes and electrons occurred in the emitting layer of device B compared with that of device A. The maximum EQE of device B was 5.9%, which was medium higher than that of many nondoped fluorescence OLEDs.^{37,38} Therefore, it is assumed that triplet excitons contributed to the device efficiencies. The EL spectrum and emission image of device B are shown in Figure 7D. The EL spectrum ($\lambda_{\text{EL}} = 517$ nm) was almost identical to the PL spectrum of TBC-10 film ($\lambda_{\text{PL}} = 511$ nm) (Figure 6B), suggesting efficient energy transfer from the host moieties to the guest moieties in the emitting layer of device B. The device B performance was higher than nondoped OLEDs using self-host-type green TADF polymers (Table S1), although it was moderate compared with nondoped OLEDs using other self-host TADF emitters.³⁰ Thus, the devices based on TBC-10 as the emitting layer, fabricated by a solution-processing method, showed good performance.

CONCLUSIONS

TADF benzyl cellulose derivatives (TBC-X), which contained both host moieties (Cz groups) and guest moieties (BCz-PI groups) through ester linkages in the molecule, were synthesized from BnC and had good solubility and film-forming properties. Indeed, the TBC-X spin-coated films could be fabricated on various substrates. TBC-10 (with ratio host and guest moieties of 93 and 7, respectively) film had the

highest PLQY (55.3%) among the TBC-X films. Transient PL decay measurements also confirmed that the TBC-10 film had TADF characteristics. Finally, devices A and B based on TBC-10 in a solution-processed emitting layer were fabricated. The EL spectrum of device B indicated efficient energy transfer from the host moieties to the guest moieties of TBC-10 in the emitting layer, and green emission was also observed in device B. Consequently, TBC-X is the first cellulose-based self-host-type TADF pendant polymer and has great promise as a material toward biodegradable nondoped OLEDs.

ASSOCIATED CONTENT

Supporting Information

The Supporting Information is available free of charge at <https://pubs.acs.org/doi/10.1021/acs.macromol.9b02644>.

¹H NMR spectra, ¹³C NMR spectra, FT-IR spectra, AFM images, DSC curves, UV–vis spectra and cyclic voltammograms of the synthetic compounds, and the current and power efficiency vs current density characteristics of the devices (PDF)

AUTHOR INFORMATION

Corresponding Author

Toshiyuki Takano – Division of Forest and Biomaterials Science, Graduate School of Agriculture, Kyoto University, Uji, Kyoto 606-8502, Japan; orcid.org/0000-0001-8244-223X; Email: takatmys@kais.kyoto-u.ac.jp

Authors

Masaya Shibano – Division of Forest and Biomaterials Science, Graduate School of Agriculture, Kyoto University, Uji, Kyoto 606-8502, Japan

Hiroki Ochiai – Division of Forest and Biomaterials Science, Graduate School of Agriculture, Kyoto University, Uji, Kyoto 606-8502, Japan

Katsuaki Suzuki – Institute for Chemical Research, Kyoto University, Uji, Kyoto 611-0011, Japan; orcid.org/0000-0001-8042-9517

Hiroshi Kamitakahara – Division of Forest and Biomaterials Science, Graduate School of Agriculture, Kyoto University, Uji, Kyoto 606-8502, Japan; orcid.org/0000-0002-0130-1919

Hironori Kaji – Institute for Chemical Research, Kyoto University, Uji, Kyoto 611-0011, Japan; orcid.org/0000-0002-5111-3852

Complete contact information is available at:

<https://pubs.acs.org/doi/10.1021/acs.macromol.9b02644>

Author Contributions

M.S., H.O., and K.S. contributed equally to the work. (M.S. designed this work and contributed to the preparation and characterization of low molecular compounds; H.O. contributed to the preparation and characterization of TBC-X; K.S. contributed to the fabrication and evaluation of the devices.) H.K. supported the synthesis and characterization of compounds. H.K. planned and supervised the device part of this study. T.T. supervised the material part of this study. M.S. wrote the manuscript with T.T.

Notes

The authors declare no competing financial interest.

ACKNOWLEDGMENTS

This work was supported by Grant-in-Aid for JSPS Fellows (Grant 16J11528) and JSPS Grand-in-Aid for Scientific Research (A) (17H01231) in Japan.

REFERENCES

- (1) Zhu, H.; Luo, W.; Ciesielski, P. N.; Fang, Z.; Zhu, J. Y.; Henriksson, G.; Himmel, M. E.; Hu, L. Wood-Derived Materials for Green Electronics, Biological Devices and Energy Applications. *Chem. Rev.* **2016**, *116*, 9305–9374.
- (2) Zhu, H.; Xiao, Z.; Liu, D.; Li, Y.; Weadock, N. J.; Fang, Z.; Huang, J.; Hu, L. Biodegradable transparent substrates for flexible organic-light-emitting diodes. *Energy Environ. Sci.* **2013**, *6*, 2105–2111.
- (3) Purandare, S.; Gomez, E. F.; Steckl, A. J. High brightness phosphorescent organic light emitting diodes on transparent and flexible cellulose films. *Nanotechnology* **2014**, *25*, 094012.
- (4) Tong, R.; Chen, G.; Tian, J.; He, M. Highly transparent, weakly hydrophilic and biodegradable cellulose film for flexible electroluminescent devices. *Carbohydr. Polym.* **2020**, *227*, 115366.
- (5) Sakakibara, K.; Ogawa, Y.; Nakatsubo, F. First cellulose Langmuir-Blodgett films towards photocurrent generation systems. *Macromol. Rapid Commun.* **2007**, *28*, 1270–1275.
- (6) Saito, Y.; Kamitakahara, H.; Takano, T. Preparation of a squaraine-bounded cellulose derivative for photocurrent generation system. *Carbohydr. Res.* **2016**, *421*, 40–45.
- (7) Saito, Y.; Kamitakahara, H.; Takano, T. Preparation of (ruthenium (II) complex)-bound cellulose derivative for photocurrent generation system. *J. Wood Sci.* **2016**, *62*, 270–275.
- (8) Saito, Y.; Kamitakahara, H.; Takano, T. Preparation of phthalocyanine-bound myristoyl celluloses for photocurrent generation system. *Cellulose* **2017**, *24*, 3659–3669.
- (9) Karakawa, M.; Chikamatsu, M.; Nakamoto, C.; Maeda, Y.; Kubota, S.; Yase, K. Organic Light-Emitting Diode Application of Fluorescent Cellulose as a Natural Polymer. *Macromol. Chem. Phys.* **2007**, *208*, 2000–2006.
- (10) Lee, S. Y.; Yasuda, T.; Nomura, H.; Adachi, C. High-efficiency organic light-emitting diodes utilizing thermally activated delayed fluorescence from triazine-based donor-acceptor hybrid molecules. *Appl. Phys. Lett.* **2012**, *101*, 093306.
- (11) Uoyama, H.; Goushi, K.; Shizu, K.; Nomura, H.; Adachi, C. Highly efficient organic light-emitting diodes from delayed fluorescence. *Nature* **2012**, *492*, 234–238.
- (12) Adachi, C. Third-generation organic electroluminescence materials. *Jpn. J. Appl. Phys.* **2014**, *53*, 060101.
- (13) Baldo, M. A.; O'Brien, D. F.; Thompson, M. E.; Forrest, S. R. Excitonic Singlet-Triplet Ratio in a Semiconducting Organic Thin Film. *Phys. Rev. B: Condens. Matter Mater. Phys.* **1999**, *60*, 14422–14428.
- (14) Shizu, K.; Noda, H.; Tanaka, H.; Taneda, M.; Uejima, M.; Sato, T.; Tanaka, K.; Kaji, H.; Adachi, C. Highly Efficient Blue Electroluminescence Using Delayed-Fluorescence Emitters with Large Overlap Density between Luminescent and Ground States. *J. Phys. Chem. C* **2015**, *119*, 26283–26289.
- (15) Kaji, H.; Suzuki, H.; Fukushima, T.; Shizu, K.; Suzuki, K.; Kubo, S.; Komino, T.; Oiwa, H.; Suzuki, F.; Wakamiya, A.; Murata, Y.; Adachi, C. Purely organic electroluminescent material realizing 100% conversion from electricity to light. *Nat. Commun.* **2015**, *6*, 1–8.
- (16) Yang, Z.; Mao, Z.; Xie, Z.; Zhang, Y.; Liu, S.; Zhao, J.; Xu, J.; Chi, Z.; Aldred, M. P. Recent advances in organic thermally activated delayed fluorescence materials. *Chem. Soc. Rev.* **2017**, *46*, 915–1016.
- (17) Wada, Y.; Shizu, K.; Kubo, S.; Suzuki, K.; Tanaka, H.; Adachi, C.; Kaji, H. Highly efficient electroluminescence from a solution-processable thermally activated delayed fluorescence emitter. *Appl. Phys. Lett.* **2015**, *107*, 183303.
- (18) Suzuki, K.; Adachi, C.; Kaji, H. Solution-processable thermally activated delayed fluorescence emitters for application in organic light emitting diodes. *J. Soc. Inf. Dispersion* **2017**, *25*, 480–485.
- (19) Zou, Y.; Gong, S.; Xie, G.; Yang, C. Design Strategy for Solution-Processable Thermally Activated Delayed Fluorescence Emitters and Their Applications in Organic Light-Emitting Diodes. *Adv. Opt. Mater.* **2018**, *6*, 1800568.
- (20) Wada, Y.; Kubo, S.; Kaji, H. Adamantyl Substitution Strategy for Realizing Solution-Processable Thermally Stable Deep-Blue Thermally Activated Delayed Fluorescence Materials. *Adv. Mater.* **2018**, *30*, 1705641.
- (21) Huang, T.; Jiang, W.; Duan, L. Recent progress in solution processable TADF materials for organic light-emitting diodes. *J. Mater. Chem. C* **2018**, *6*, 5577–5596.
- (22) Luo, J.; Gong, S.; Gu, Y.; Chen, T.; Li, Y.; Zhong, C.; Xie, G.; Yang, C. Multi-carbazole encapsulation as a simple strategy for the construction of solution-processed, non-doped thermally activated delayed fluorescence emitters. *J. Mater. Chem. C* **2016**, *4*, 2442–2446.
- (23) Ban, X.; Jiang, W.; Lu, T.; Jing, X.; Tang, Q.; Huang, S.; Sun, K.; Huang, B.; Lin, B.; Sun, Y. Self-host thermally activated delayed fluorescent dendrimers with flexible chains: an effective strategy for non-doped electroluminescent devices based on solution processing. *J. Mater. Chem. C* **2016**, *4*, 8810–8816.
- (24) Ban, X.; Jiang, W.; Sun, K.; Lin, B.; Sun, Y. Self-Host Blue Dendrimer Composed of Thermally Activated Delayed Fluorescence Core and Bipolar Dendrons for Efficient Solution-Processable Nondoped Electroluminescence. *ACS Appl. Mater. Interfaces* **2017**, *9*, 7339–7346.
- (25) Ban, X.; Zhu, A.; Zhang, T.; Tong, Z.; Jiang, W.; Sun, Y. Highly Efficient All-Solution-Processed Fluorescent Organic Light-Emitting Diodes Based on a Novel Self-Host Thermally Activated Delayed Fluorescence Emitter. *ACS Appl. Mater. Interfaces* **2017**, *9*, 21900–21908.
- (26) Zeng, X.; Luo, J.; Zhou, T.; Chen, T.; Zhou, X.; Wu, K.; Zou, Y.; Xie, G.; Gong, S.; Yang, C. Using Ring-Opening Metathesis Polymerization of Norbornene To Construct Thermally Activated Delayed Fluorescence Polymers: High-Efficiency Blue Polymer Light-Emitting Diodes. *Macromolecules* **2018**, *51*, 1598–1604.
- (27) Li, C.; Wang, Y.; Sun, D.; Li, H.; Sun, X.; Ma, D.; Ren, Z.; Yan, S. Thermally Activated Delayed Fluorescence Pendant Copolymers with Electron- and Hole-Transporting Spacers. *ACS Appl. Mater. Interfaces* **2018**, *10*, 5731–5739.
- (28) Li, C.; Ren, Z.; Sun, X.; Li, H.; Yan, S. Deep-Blue Thermally Activated Delayed Fluorescence Polymers for Nondoped Solution-Processed Organic Light-Emitting Diodes. *Macromolecules* **2019**, *52*, 2296–2303.
- (29) Park, Y. H.; Jang, H. J.; Lee, J. Y. High efficiency above 20% in polymeric thermally activated delayed fluorescent organic light-emitting diodes by a host embedded backbone structure. *Polym. Chem.* **2019**, *10*, 4872–4878.
- (30) Godumala, M.; Choi, S.; Cho, M. J.; Choi, D. H. Recent breakthroughs in thermally activated delayed fluorescence organic light emitting diodes containing non-doped emitting layers. *J. Mater. Chem. C* **2019**, *7*, 2172–2198.
- (31) Tsai, M.-H.; Hong, Y.-H.; Chang, C.-H.; Su, H.-C.; Wu, C.-C.; Matoliukstyte, A.; Simokaitiene, J.; Grigalevicius, S.; Grazulevicius, J. V.; Hsu, C.-P. 3-(9-Carbazolyl)carbazoles and 3,6-Di(9-carbazolyl)-carbazoles as Effective Host Materials for Efficient Blue Organic Electrophosphorescence. *Adv. Mater.* **2007**, *19*, 862–866.
- (32) Li, M.; Liu, Y.; Duan, R.; Wei, X.; Yi, Y.; Chen, C.-F. Aromatic-Imide-Based Thermally Activated Delayed Fluorescence Materials for Highly Efficient Organic Light-Emitting Diodes. *Angew. Chem., Int. Ed.* **2017**, *56*, 8818–8822.
- (33) Gómez, J. A. C.; Erlar, U. W.; Klemm, D. O. 4-methoxy substituted trityl groups in 6-O protection of cellulose: Homogeneous synthesis, characterization, detritylation. *Macromol. Chem. Phys.* **1996**, *197*, 953–964.

(34) Harkness, B. R.; Gray, D. G. Preparation and chiroptical properties of tritylated cellulose derivatives. *Macromolecules* **1990**, *23*, 1452–1457.

(35) Geng, Y.; Cui, L.-S.; Kim, J. U.; Nakanotani, H.; Adachi, C. Molecular Design for Blue Thermal Activated Delayed Fluorescence Materials: Substitution Position Effect. *Chem. Lett.* **2017**, *46*, 1490–1492.

(36) Suzuki, K.; Kubo, S.; Shizu, K.; Fukushima, T.; Wakamiya, A.; Murata, Y.; Adachi, C.; Kaji, H. Triarylboron-Based Fluorescent Organic Light-Emitting Diodes with External Quantum Efficiencies Exceeding 20%. *Angew. Chem., Int. Ed.* **2015**, *54*, 15231–15235.

(37) Zhu, X.-H.; Peng, J.; Cao, Y.; Roncali, J. Solution-processable single-material molecular emitters for organic light-emitting devices. *Chem. Soc. Rev.* **2011**, *40*, 3509–3524.

(38) Rizzo, F.; Cucinotta, F. Recent Developments in AIEgens for Non-Doped and TADF OLEDs. *Isr. J. Chem.* **2018**, *58*, 874–888.

(39) Luo, J.; Xie, G.; Gong, S.; Chen, T.; Yang, C. Creating a thermally activated delayed fluorescence channel in a single polymer system to enhance exciton utilization efficiency for bluish-green electroluminescence. *Chem. Commun.* **2016**, *52*, 2292–2295.